FREQUENCY-DOMAIN WEIGHTED-AVERAGING FINITE-DIFFERENCE NUMERICAL SIMULATION OF qP WAVE PROPAGATION IN TTI MEDIA

GUOCHEN WU, KAI LIANG and XINGYAO YIN

College of Geo-Resources and Information, China University of Petroleum (East China), Beier Road #271, Dongying, Shan Dong 257061, P.R. China.
guochenwu@upc.edu.cn

(Received August 6, 2009; revised version accepted March 10, 2010)

ABSTRACT

Wu, G., Liang, K. and Yin, X., 2010. Frequency-domain weighted-averaging finite-difference numerical simulation of qP wave propagation in TTI media. *Journal of Seismic Exploration*, 19: 207-229.

The finite-difference method is widely used in numerical simulation of the propagation of seismic waves, but has the limitation that numerical dispersion reduces the accuracy and resolution of seismic wavefield simulation. In order to decrease the numerical dispersion of conventional finite-difference operators, this paper presents a frequency-domain weighted-averaging finite-difference operators defined on a 25-point stencil for numerical simulation of qP waves propagating in transversely isotropic media with a tilted symmetry axis (TTI media). We first approximate the differential operators using finite-difference analogues defined on 25-point stencils and then calculate the weighted average of the difference operators with weighting coefficients. The weighting coefficients are determined by the Gauss-Newton method of optimization theory. Using the weighted-averaging finite-difference analogues and combined boundary conditions, we successfully simulate qP wave propagation in homogeneous TTI media, layered TTI media and VTI Salt model. The seismic wavefields in the time and frequency domains are obtained and used to generate single shot records. The result of numerical simulation indicates that 25-point weighted-averaging finite-difference analogues can improve the accuracy of the numerical simulation of wavefields and efficiently suppress the numerical dispersion of conventional difference operators. This method may be employed in the foundation of qP migration and inversion in TTI media.

KEYWORDS: TTI media, weighted-averaging, finite-difference, weighting coefficients, numerical dispersion.

0963-0651/10/$5.00

INTRODUCTION

The finite-difference method is a widely applied method for seismic numerical simulation. It can accurately simulate seismic wave propagation in an inhomogeneous medium, but this accuracy may be limited by numerical dispersion. In order to decrease the numerical dispersion, researchers have presented many correlative methods. To solve the 2D acoustic equation in isotropic media, Jo et al. (1996) presented an optimal 9-point weighted-averaging method. To improve the accuracy of finite-difference operators, Shin and Sohn (1998) designed a 25-point weighted-averaging operator defined on a 25-point stencil and based on four different angles. Some researchers have applied the optimal weighted-averaging finite-difference operators to frequency-domain forward modeling in isotropic media. Štekl and Pratt (1998) presented 9-point finite-difference operators which are calculated in rotated coordinate systems. Min et al. (2000) proposed a weighted-averaging scheme on a 25-point stencil for 2D elastic modeling in the frequency domain, and developed a weighted-averaging finite-element method for forward modeling of the acoustic wave equation (2002) and 2D elastic wave equations (2003) in the frequency domain.

Based on that earlier work, this paper extends the frequency-domain weighted-averaging finite-difference numerical simulation method from isotropic media to TTI media, and presents frequency-domain weighted-averaging finite-difference operators defined on a 25-point stencil for qP wave simulation in TTI media. Using the weighted-averaging finite-differences on a 25-point stencil, we have successfully simulated qP wave propagation in homogeneous TTI media, layered TTI media and in a complex VTI model.

WEIGHTED-AVERAGING FINITE-DIFFERENCE METHOD

In order to simulate qP wave propagation in VTI media and orthorhombic anisotropic media (OA media), Alkhalifah (1998, 2000, 2003) proposed an acoustic approximation and obtained a qP wave equation. Zhang et al. (2003) applied the acoustic approximation for VTI media and OA media to TTI media. The 2D frequency-domain approximate qP wave equation in a homogeneous TTI media is given by (Zhang et al., 2003)

$$\omega^4 F + A\omega^2 V_{P0}^2(\partial^2 F/\partial x^2) + B\omega^2 V_{P0}^2(\partial^2 F/\partial z^2) + C\omega^2 V_{P0}^2(\partial^2 F/\partial x \partial z)$$

$$+ DV_{P0}^4(\partial^4 F/\partial x^2 \partial z^2) + EV_{P0}^4(\partial^4 F/\partial x^4) + GV_{P0}^4(\partial^4 F/\partial z^4)$$

$$+ HV_{P0}^4(\partial^4 F/\partial x^3 \partial z) + IV_{P0}^4(\partial^4 F/\partial x \partial z^3) = 0 \quad , \qquad (1)$$

where

$$A = (\chi\cos^2\theta^0 + \sin^2\theta^0),\ B = (\chi\sin^2\theta^0 + \cos^2\theta^0),\ C = (1 - \chi)\sin2\theta^0,$$

$$D = (2 - 3\sin^2 2\theta^0)\eta,\ E = \tfrac{1}{2}\eta\sin^2 2\theta^0,\ G = \tfrac{1}{2}\eta\sin^2 2\theta^0,\ H = -\eta\sin4\theta^0$$

and $I = \eta\sin4\theta^0$.

In eq. (1), $\chi = 1 + 2\epsilon$ and $\eta = \epsilon - \delta$ are anisotropic parameters, F is the wavefield in the frequency domain, ω is the angular frequency, ρ is the density, and V_{P0} is the qP wave propagation velocity along to the symmetry axis in TTI media, ϵ and δ are dimensionless anisotropic parameters (Thomson, 1986) and θ^0 is the angle between symmetry axis of the TTI media and the vertical axis.

After discretization of the qP wave equation in TTI media, the wave field $F_{i,j}$ is assumed to be specified on the grid (i,j) where i and j represent the z- and x-directions, respectively. The conventional finite difference analogues approximating the related differential operators are given by eq. (2), and the conventional finite difference schemes are shown in Fig. 1.

$$\begin{aligned}
\partial^2F/\partial x^2 &\approx (1/\Delta x^2)(F_{i,j+1} - 2F_{i,j} + F_{i,j-1}) \ , \\
\partial^2F/\partial z^2 &\approx (1/\Delta z^2)(F_{i+1,j} - 2F_{i,j} + F_{i-1,j}) \ , \\
\partial^2F/\partial x\partial z &\approx (1/4\Delta x\Delta z)(F_{i+1,j+1} - F_{i+1,j-1} - F_{i-1,j+1} + F_{i-1,j-1}) \ , \\
\partial^4F/\partial x^2\partial z^2 &\approx (1/\Delta x^2\Delta z^2)[4F_{i,j} - 2(F_{i+1,j} + F_{i,j+1} + F_{i,j-1} + F_{i-1,j}) \\
&\quad + F_{i+1,j+1} + F_{i+1,j-1} + F_{i-1,j+1} + F_{i-1,j-1}] \ , \\
\partial^4F/\partial x^4 &\approx (1/\Delta x^4)(F_{i,j+2} - 4F_{i,j+1} + 6F_{i,j} - 4F_{i,j-1} + F_{i,j-2}) \ , \\
\partial^4F/\partial z^4 &\approx (1/\Delta z^4)(F_{i+2,j} - 4F_{i+1,j} + 6F_{i,j} - 4F_{i-1,j} + F_{i-2,j}) \ .
\end{aligned} \tag{2}$$

The above are second central finite difference for approximation of $(\partial^2F/\partial x^2)$ or $(\partial^2F/\partial z^2)$, second-order or fourth-order mixed difference operator for approximation of $(\partial^2F/\partial x\partial z)$ or $(\partial^4F/\partial x^2\partial z^2)$ and fourth-order difference operator for approximation of $(\partial^4F/\partial x^4)$ or $(\partial^4F/\partial z^4)$.

Because conventional difference schemes use information of few grids, the numerical simulation has low accuracy and serious numerical dispersion. To improve the accuracy of finite-difference operators, this paper presents frequency-domain weighted-averaging finite-differences on 25-point stencils for

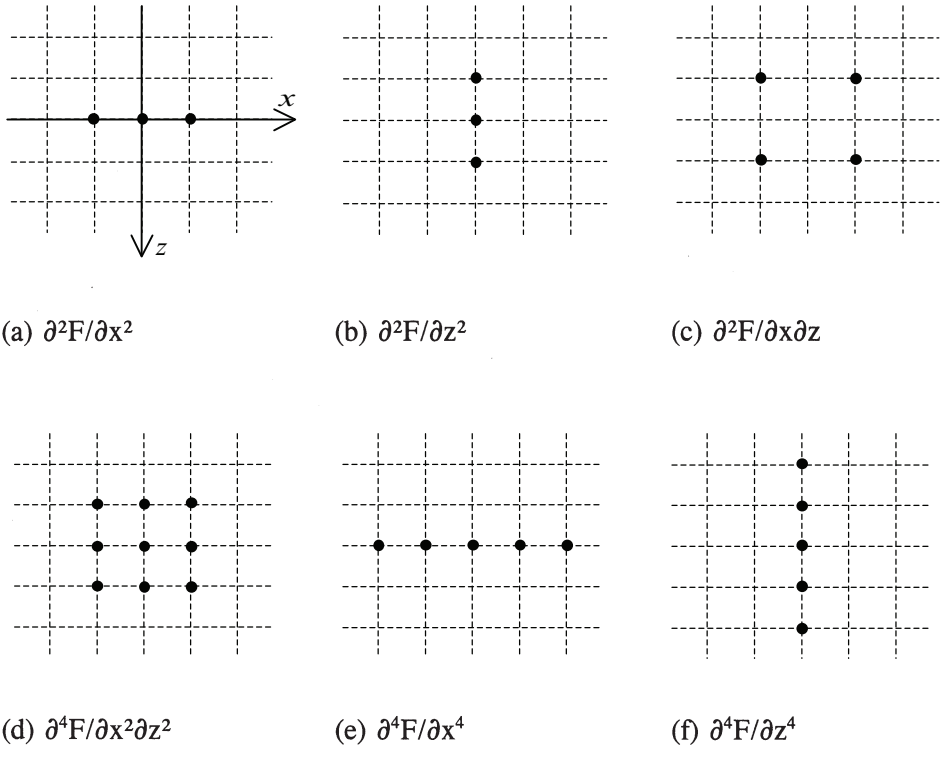

Fig. 1. Computational grids used to approximate differential operators by the conventional scheme for (a) ($\partial^2F/\partial x^2$), (b) ($\partial^2F/\partial z^2$), (c) ($\partial^2F/\partial x\partial z$), (d) ($\partial^4F/\partial x^2\partial z^2$), (e) ($\partial^4F/\partial x^4$) and (f) ($\partial^4F/\partial z^4$). The above are second central finite differences for approximation of ($\partial^2F/\partial x^2$) or ($\partial^2F/\partial z^2$), second-order or fourth-order mixed difference operator for approximation of ($\partial^2F/\partial x\partial z$) or ($\partial^4F/\partial x^2\partial z^2$), fourth-order difference operator for approximation of ($\partial^4F/\partial x^4$) or ($\partial^4F/\partial z^4$).

numerical simulation of qP wave propagation in TTI media. The method approximates the differential operators using finite-difference analogues defined on 25-point stencils and then averages the analogues with different weighting coefficients.

The weighted-averaging finite-difference operators of $\partial^2F/\partial x^2$, $\partial^2F/\partial z^2$, $\partial^2F/\partial x\partial z$ and $F_{i,j}$ were developed by Min et al. (2000) (see Fig. 2). Fig. 2a shows weighted-averaging scheme on 25-point stencils for $\partial^2F/\partial x^2$. Formulate two second central difference operators using five grid points in each row, which are averaged with the weighting coefficients c (for points) and d (for circles). Applying the same processing to all five rows, we obtain five difference operators and average them with weighting coefficients b_1,b_2,b_3 (see Fig. 2a). A similar scheme is applied to the approximation of $\partial^2F/\partial z^2$ (see Fig. 2b). Average the finite-difference operators with weighting coefficients e_1 (for points in Fig. 2c) and f_1 (for circles) in the approximation of $\partial^2F/\partial x\partial z$ (Fig. 2c).

The wavefield $F_{i,j}$ at the collocation point is averaged with weighting coefficients a_1,a_2,a_3,a_4,a_5,a_6 (see Fig. 2d). The finite-difference analogues of the differential operators $\partial^2F/\partial x^2$, $\partial^2F/\partial z^2$, $\partial^2F/\partial x\partial z$ and $F_{i,j}$ are given by Min et al. (2000) as

$$\partial^2F/\partial x^2 \approx \sum (b_{|l|+1}/\Delta x^2)[c(F_{i+l,j+1} - 2F_{i+l,j} + F_{i+l,j-1}) + (d/4)(F_{i+l,j+2} - 2F_{i+l,j} + F_{i+l,j-2})] \quad , \tag{3}$$

$$\partial^2F/\partial z^2 \approx \sum (b_{|l|+1}/\Delta z^2)[c(F_{i+1,j+l} - 2F_{i+j,l} + F_{i+1,j-l}) + (d/4)(F_{i+2,j+l} - 2F_{i,j+l} + F_{i-2,j+l})] \quad , \tag{4}$$

for $l = -2,-1,0,1,2,$

$$\partial^2F/\partial x\partial z \approx (e_1/4\Delta x\Delta z)(F_{i+1,j+1} - F_{i+1,j-1} - F_{i-1,j+1} + F_{i-1,j-1}) + (f_1/16\Delta x\Delta z)(F_{i+2,j+2} - F_{i+2,j-2} - F_{i-2,j+2} + F_{i-2,j-2}) \quad , \tag{5}$$

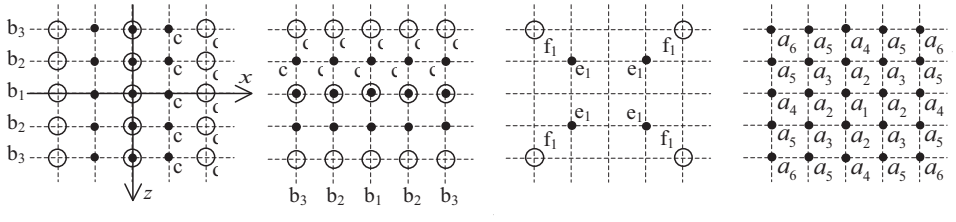

(a) $\partial^2F/\partial x^2$ (b) $\partial^2F/\partial z^2$ (c) $\partial^2F/\partial x\partial z$ (d) $F_{i,j}$

Fig. 2. Computational grids used to approximate differential operators by the weighted-averaging scheme on 25-point stencils for (a) ($\partial^2F/\partial x^2$), (b) ($\partial^2F/\partial z^2$), (c) ($\partial^2F/\partial x\partial z$) and (d) $F_{i,j}$. To appropriate ($\partial^2F/\partial x^2$) or ($\partial^2F/\partial z^2$), formulate two second central difference operators using five grid points in each row or column, which are averaged with the weighting coefficients c (for points) and d (for circles). Applying the same processing to all five rows or columns, we obtain five difference operators and average them with weighting coefficients b_1,b_2,b_3. Average the finite-difference operators with weighting coefficients e_1 (for points in Fig. 2c) and f_1(for circles) in the approximation of $\partial^2F/\partial x\partial z$. The wavefield $F_{i,j}$ at collocation point is averaged with weighting coefficients a_1,a_2,a_3,a_4,a_5,a_6 (Min et al., 2000).

$$F_{i,j} \approx a_1F_{i,j} + a_2(F_{i+1,j} + F_{i,j+1} + F_{i,j-1} + F_{i-1,j}) + a_3(F_{i+1,j+1} + F_{i+1,j-1} + F_{i-1,j+1} + F_{i-1,j-1}) + a_4(F_{i+2,j} + F_{i,j+2} + F_{i,j-2} + F_{i-2,j}) + a_5(F_{i+2,j+1} + F_{i+2,j-1} + F_{i+1,j+2} + F_{i+1,j-2} + F_{i-1,j+2} + F_{i-1,j-2} + F_{i-2,j+1} + F_{i-2,j-1}) + a_6(F_{i+2,j+2} + F_{i+2,j-2} + F_{i-2,j+2} + F_{i-2,j-2}) \quad . \tag{6}$$

The weighted-averaging analogue defined on a 25-point stencil is introduced into the difference operator $\partial^4F/\partial x^2\partial z^2$ (Wu and Liang, 2005). Two finite-difference operators are formulated, both of which are 9 term fourth-order mixed difference operator. The interval of one difference operator (points in Fig. 3) is Δx and Δz, the interval of the other (circles in Fig. 3) is $2\Delta x$ and $2\Delta z$. The two finite-difference analogues are averaged with the weighting coefficients e_2 (for points) and f_2 (for circles). The finite-difference analogue of $\partial^4F/\partial x^2\partial z^2$ is given by

$$\partial^2F/\partial x^2\partial z^2 \approx (e_2/\Delta x^2\Delta z^2)(F_{i+1,j+1} - 2F_{i+1,j} + F_{i+1,j-1} - 2F_{i,j+1} + 4F_{i,j} - 2F_{i,j-1} + F_{i-1,j+1} - 2F_{i-1,j} + F_{i-1,j-1}) + (f_2/16\Delta x^2\Delta z^2)(F_{i+2,j+2} - 2F_{i+2,j} + F_{i+2,j-2} - 2F_{i,j+2} + 4F_{i,j} - 2F_{i,j-2} + F_{i-2,j+2} - 2F_{i-2,j} + F_{i-2,j-2}) \quad . \tag{7}$$

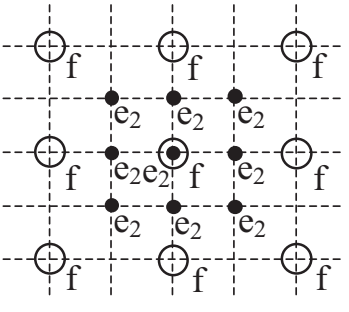

Fig. 3. Computational grids used to approximate differential operators by the weighted-averaging scheme on 25-point stencils for $\partial^4F/\partial x^2\partial z^2$. Two finite-difference operators are formulated, both of which are 9 item fourth-order mixed difference operators. The interval of one difference operator (for points) is Δx and Δz, the interval of the other (for circles) is $2\Delta x$ and $2\Delta z$. The two finite-difference operators are averaged with the weighting coefficients e_2 (for points) and f^2 (for circles).

The weighted-averaging analogues defined on 25-point stencils are introduced into other difference terms. For $\partial^4F/\partial x^4$, we formulate a conventional fourth-order finite-difference analogue in each row, then average them with weighting coefficients g_1,g_2,g_3 (see Fig. 4a). The weighting coefficient g_1 is used for the third row, g_2 for the second and the fourth row, and g_3 for the first and the fifth row. A similar scheme is applied to the approximation of $\partial^2F/\partial z^4$ (see Fig. 4b). For $\partial^4F/\partial x^3\partial z$ and $\partial^4F/\partial x\partial z^3$, average difference analogues with weighting coefficients h (see Fig. 4c and Fig. 4d). The finite-difference analogues of $\partial^4F/\partial x^4$, $\partial^4F/\partial z^4$, $\partial^4F/\partial x^3\partial z$ and $\partial^4F/\partial x\partial z^3$ are given by

$$\partial^2F/\partial x^4 \approx \sum (g_{|l|+1}/\Delta x^4)(F_{i+l,j+2} - 4F_{i+l,j+1} + 6F_{i+l,j} - 4F_{i+l,j-1} + F_{i+l,j-2}) \quad , \tag{8}$$

$$\partial^2F/\partial z^4 \approx \sum (g_{|l|+1}/\Delta z^4)(F_{i+2,j+l} - 4F_{i+1,j+l} + 6F_{i,j+l} - 4F_{i-1,j+l} + F_{i-2,j+l}) \quad , \tag{9}$$

for $l = -2,-1,0,1,2,$

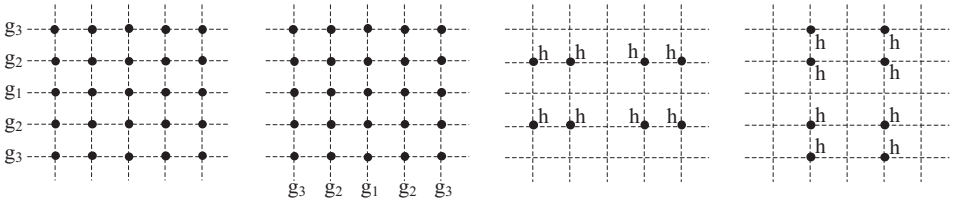

(a) $\partial^4F/\partial x^4$ (b) $\partial^4F/\partial z^4$ (c) $\partial^4F/\partial x^3\partial z$ (d) $\partial^4F/\partial x\partial z^3$

Fig. 4. Computational grids used to approximate differential operators by the weighted-averaging scheme on 25-point stencils for (a) ($\partial^4F/\partial x^4$), (b) ($\partial^4F/\partial z^4$), (c) ($\partial^4F/\partial x^3\partial z$) and (d) ($\partial^4F/\partial x\partial z^3$). For $\partial^4F/\partial x^4$, we formulate a conventional fourth-order finite-difference operator in each of five rows, then average them with weighting coefficients g_1,g_2,g_3. The weighting coefficient g_1 is used for the third row, g_2 for the second and the fourth row, and g_3 for the first and the fifth row. A similar scheme is applied to the approximation of $\partial^2F/\partial z^4$. For $\partial^4F/\partial x^3\partial z$ and $\partial^4F/\partial x\partial z^3$, average difference analogues with weighting coefficients h.

$$\partial^4 F/\partial x^3\partial z \approx (h/4\Delta x^3\Delta z)(F_{i+1,j+2} - 2F_{i+1,j+1} + 2F_{i+1,j-1} - F_{i+1,j-2} - F_{i-1,j+2} + 2F_{i-1,j+1} - 2F_{i-1,j-1} + F_{i-1,j-2}) \quad , \tag{10}$$

$$\partial^4 F/\partial x\partial z^3 \approx (h/4\Delta x\Delta z^3)(F_{i+2,j+1} - F_{i+2,j-1} - 2F_{i+1,j+1} + 2F_{i+1,j-1} + 2F_{i-1,j+1} - 2F_{i-1,j-1} - F_{i-2,j+1} + F_{i-2,j-1}) \quad . \tag{11}$$

Substituting eqs. (3)-(11) into eq. (1), the 2D frequency-domain difference equation for the qP wave is

$$\begin{aligned} &A^{12}_{i+2,j+2}F_{i+2,j+2} + A^{11}_{i+2,j+1}F_{i+2,j+1} + A^{10}_{i+2,j}F_{i+2,j} + A^{9}_{i+2,j-1}F_{i+2,j-1} \\ &+ A^{8}_{i+2,j-2}F_{i+2,j-2} + A^{7}_{i+1,j+2}F_{i+1,j+2} + A^{6}_{i+1,j+1}F_{i+1,j+1} + A^{5}_{i+1,j}F_{i+1,j} \\ &+ A^{4}_{i+1,j-1}F_{i+1,j-1} + A^{3}_{i+1,j-2}F_{i+1,j-2} + A^{2}_{i,j+2}F_{i,j+2} + A^{1}_{i,j+1}F_{i,j+1} \\ &+ A^{0}_{i,j}F_{i,j} + A^{1}_{i,j-1}F_{i,j-1} + A^{2}_{i,j-2}F_{i,j-2} + A^{3}_{i-1,j+2}F_{i-1,j+2} \\ &+ A^{4}_{i-1,j+1}F_{i-1,j+1} + A^{5}_{i-1,j}F_{i-1,j} + A^{6}_{i-1,j-1}F_{i-1,j-1} + A^{7}_{i-1,j-2}F_{i-1,j-2} \\ &+ A^{8}_{i-2,j+2}F_{i-2,j+2} + A^{9}_{i-2,j+1}F_{i-2,j+1} + A^{10}_{i-2,j}F_{i-2,j} + A^{11}_{i-2,j-1}F_{i-2,j-1} \\ &+ A^{12}_{i-2,j-2}F_{i-2,j-2} = 0 \quad . \end{aligned} \tag{12}$$

This is the difference equation at the collocation point $F_{i,j}$ using the weighted-averaging operators defined on a 25-point stencil (see details of eq. (12) in the Appendix). Such difference equations are obtained for each collocation point. Introducing the body force vector $\mathbf{G}$, we get the matrix equation (see details in the appendix)

$$\mathbf{A}_{N\times N}\mathbf{F} = \mathbf{G} \quad . \tag{13}$$

Solving eq. (13), we obtain the wavefield in the frequency domain. Transforming the wavefield from the frequency domain to time domain using a Fourier transform, snapshots in time-domain and synthetic seismograms for qP wave propagation in a TTI media are obtained.

DETERMINATION OF WEIGHTING COEFFICIENTS

For the numerical simulation for qP wave propagation in TTI media using weighted-averaging finite differences, the key is to determine the weighting coefficients. In order to minimize numerical dispersion, we determine the

optimal weighting coefficients using normalized phase velocity in TTI media, which is obtained from the dispersion relation. The weighting coefficients are determined by the Gauss-Newton method.

According to eq. (1), we obtain the finite-difference approximation equation for the homogeneous qP wave equation, from which we can obtain the dispersion relation. Substituting the weighted-averaging finite differences on a 25-point stencil and let $\Delta = \Delta x = \Delta z$, we have

$$\omega^2 = -(V_{P0}^2/2\Delta^2 P_m)AP_{xx} - (V_{P0}^2/2\Delta^2 P_m)BP_{zz} - (V_{P0}^2/2\Delta^2 P_m)CP_{xz} \pm (V_{P0}^2/2\Delta^2 P_m)\sqrt{M'} \quad , \tag{14}$$

where

$$M' = (AP_{xx} + BP_{zz} + CP_{xz})^2 - 4P_m(DP_{xxzz} + EP_{xxxx} + GP_{zzzz} + HP_{xxxz} + IP_{xzzz}) \quad .$$

The quantities P_{xx}, P_{zz}, P_{xz}, P_{xxzz}, P_{xxxx}, P_{zzzz}, P_{xxxz}, P_{xzzz}, and P_m are functions of the weighting coefficients, direction of wave propagation, and number of grid points per wavelength. θ is the angle between the direction of wave propagation and the z-axis and L is the number of grid points per wavelength. The phase velocity is defined as $V_{ph} = \omega/k$, so that the phase velocity of difference equation is

$$V_{ph}^d = [V_{P0}/2\pi(1/L)]\sqrt{[(1/2P_m)(-AP_{xx} - BP_{zz} - CP_{xz} \pm \sqrt{M''})]} \quad , \tag{15}$$

where

$$M'' = (AP_{xx} + BP_{zz} + CP_{xz})^2 - 4P_m(DP_{xxzz} + EP_{xxxx} + GP_{zzzz} + HP_{xxxz} + IP_{xzzz}) \quad .$$

Eq. (15) is the phase velocity obtained from the dispersion relation of the difference equation. The phase velocity of the wave equation is obtained in a similar manner. The dispersion relation for the qP wave equation is

$$\omega^4 - (Ak_x^2 + Bk_z^2 + Ck_xk_z)V_{P0}^2\omega^2 + (Dk_x^2k_z^2 + Ek_x^4 + Gk_z^4 + Hk_x^3k_z + Ik_xk_z^3)V_{P0}^4 = 0 \quad , \tag{16}$$

where the horizontal and vertical components of the wave vector are $k_x = k\sin\theta = \omega p_x$ and $k_z = k\cos\theta = \omega p_z$, respectively. $\mathbf{k} = (k_x\sin\theta, k_z\cos\theta) = (\omega p_x, \omega p_z)$ is the wave vector. Solving eq. (16), the phase velocity of the qP wave equation

may be written as

$$V_{ph}^{w} = V_{P0}\sqrt{\{\tfrac{1}{2}[\chi\sin^2\theta' + \cos^2\theta' \pm \sqrt{((\chi\sin^2\theta' + \cos^2\theta')^2 - 8\eta\sin^2\theta'\cos^2\theta')}]\}} \quad , \tag{17}$$

where $\theta' = \theta + \theta^0$.

We expect the phase velocity of the difference equation to be equal to that of the wave equation, so that the numerical dispersion is very low. The normalized phase velocity is defined as $f = V_{ph}^{d}/V_{ph}^{w}$. This is a non-linear optimal problem. The optimal weighting coefficients, which make the normalized phase velocity close to unity, are determined by the Gauss-Newton method (Lines and Treitel, 1984; Min et al., 2000).

The Gauss-Newton method requires the Jacobian matrix **J** (Min et al., 2000). We can construct the Jacobian matrix **J** by changing the anisotropic parameters ε and δ, the angle θ^0 between the symmetry axis of TTI media and the vertical axis, propagation angle θ, and L (number of grid points per wavelength). We change ε and δ from 0.0 to 0.3 in steps of 0.01, θ^0 from $-90°$ to 90° in 15° steps, θ from 0° to 90° in 15° steps, 1/L from 0.01 to 0.3 in steps of 0.01. The matrix **J** then becomes an overdetermined matrix.

The set of optimal weighting coefficients for weighted-averaging finite differences of the qP wave in TTI media is

$$\begin{aligned}
&a_1 = 0.41306,\ a_2 = 0.12387,\ a_3 = 0.015088,\ a_4 = -0.0017319,\\
&a_5 = 0.0031605,\ a_6 = -0.00084488,\ b_1 = 0.6021,\ b_2 = 0.1667,\\
&b_3 = -0.0010569,\ c = 0.66688,\ d = 0.38711,\ e_1 = 0.97882,\\
&f_1 = 0.0029809,\ e_2 = 0.59822,\ f_2 = 0.38236,\ g_1 = 0.61924,\\
&g_2 = 0.17461,\ g_3 = 0.0041994,\ h = 0.44051.
\end{aligned} \tag{18}$$

The set of weighting coefficients in eq. (18) is suitable for most weak anisotropic media, because we take the majority of propagation angle and weak anisotropic media into consideration when choosing the weighting coefficients. Once the weighting coefficients are determined, we can apply them to most weak anisotropic models.

DISPERSION ANALYSIS

Given the optimal weighting coefficients, the dispersion relations are analyzed by plotting phase velocities for different propagation angles, different numbers of grid points per wavelength, and different tilted angles from the symmetry axis. The qP wave phase velocities are obtained from eqs. (15) and (17).

We design models for isotropic media with $\varepsilon = \delta = 0.0$, $\theta^0 = 0°$, VTI media with $\varepsilon = 0.2$, $\delta = 0.3$, $\theta^0 = 0°$ and TTI media with $\varepsilon = 0.2$, $\delta = 0.3$, $\theta^0 = 45°$. 1/L is varied from 0.01 to 0.3 in steps of 0.01, and θ is varied from 0° to 90° in 15° steps. Fig. 5 shows the normalized phase velocity obtained using conventional difference operators for isotropic media (Fig. 5a), VTI media (Fig. 5c), TTI media (Fig. 5e), and weighted-averaging operators defined on a 25-point stencil for isotropic media (Fig. 5b), VTI media (Fig. 5d) and TTI media (Fig. 5f). For conventional difference operators, there is serious numerical dispersion of the qP wave normalized phase velocity, no matter if the media is isotropic (Fig. 5a), a VTI media (Fig. 5c) or a TTI media (Fig. 5e). For weighted-averaging difference operators defined on 25-point stencils, the qP wave normalized phase velocity is close to unity in all of the three media types (Fig. 5b, 5d and 5f). The result of dispersion analysis indicates that numerical dispersion for qP wave is greatly decreased by weighted-averaging operators defined on 25-point stencils.

NUMERICAL EXAMPLES

To examine the accuracy and efficiency of weighted-averaging operators defined on 25-point stencils, we designed a set of homogeneous media, including isotropic media, elliptical anisotropic media and TTI media A and B. The parameters of the homogeneous media are listed in Table 1. The grid dimensions of the model are 101 × 101, with spatial intervals of $\Delta x = 10$ m and $\Delta z = 10$ m. The dominant frequency of the Ricker wavelet is 40 Hz. The time sample rate is 2 ms and the source locations are near the center of the model.

Figs. 6 to 9 are the snapshots in the frequency-domain and the time-domain for isotropic media, elliptical anisotropic media and TTI media A and B, respectively, that is, monochromatic snapshots for conventional finite-difference operators (a) and weighting-averaging finite-difference operators (b), the snapshots in the time-domain for conventional finite-difference operators (c) and weighting-averaging finite-difference operators (d). In these figures, the qP wavefront in isotropic media is circular, in elliptical anisotropic media is elliptical. However, in the TTI media A and B, the qP wavefront demonstrates

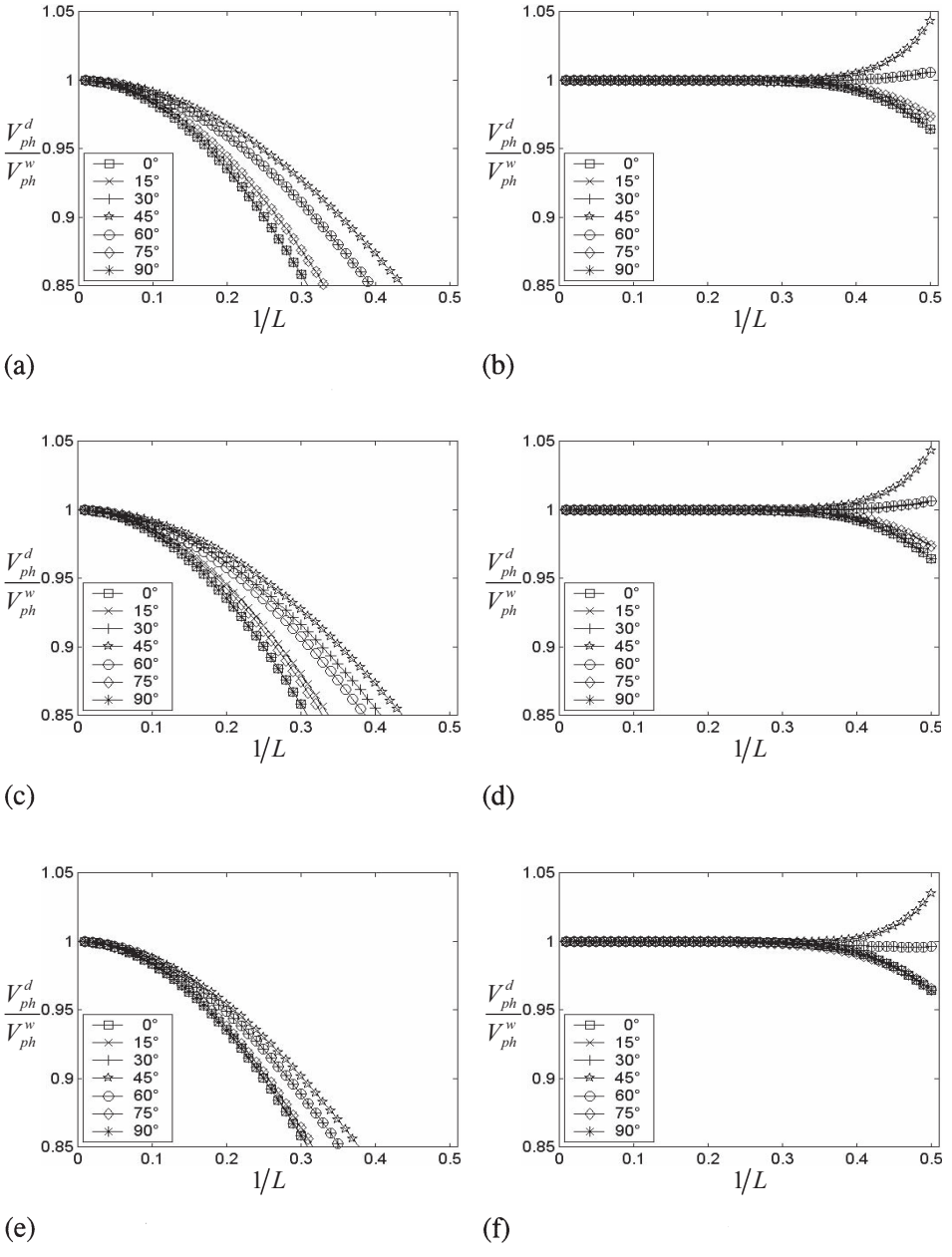

Fig. 5. Normalized phase velocity obtained using conventional difference operators (a, c, e) and weighted-averaging operators defined on a 25-point stencil (b, d, f). The models are isotropic media with $\varepsilon = \delta = 0.0$, $\theta^0 = 0°$ (a, b), VTI media with $\varepsilon = 0.2$, $\delta = 0.3$, $\theta^0 = 0°$ (c, d) and TTI media with $\varepsilon = 0.2$, $\delta = 0.3$, $\theta^0 = 45°$ (e, f). L is the number of grid points per wavelength, and propagation angle θ is varied from 0° to 90° in 15° steps.

Table 1. Parameters of the homogeneous media.

Media	V_{P0} (m/s)	ε	δ	θ^0
Isotropic media	2500	0.0	0.0	0°
Elliptical anisotropic media	2500	0.2	0.2	30°
TTI media A	2500	0.2	0.1	90°
TTI media B	2500	0.2	0.3	−45°

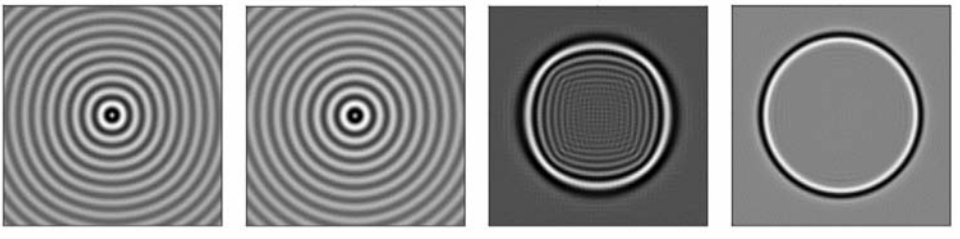

(a) (b) (c) (d)

Fig. 6. The snapshots in isotropic media. The parameters are $V_{P0} = 2500$ m/s, $\varepsilon = \delta = 0.0$, $\theta^0 = 0°$. They are the monochromatic snapshots for conventional finite-difference operators (a) and weighting-averaging finite-difference operators (b). The frequency is 40 Hz. Others are the snapshots in time-domain for conventional finite-difference operators (c) and weighting-averaging finite-difference operators (d). In these figures, the qP wavefront in isotropic media is circular.

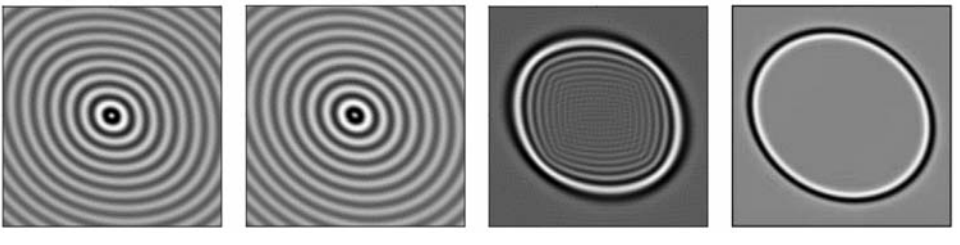

(a) (b) (c) (d)

Fig. 7. The snapshots in elliptical anisotropic media. The parameters are $V_{P0} = 2500$ m/s, $\varepsilon = \delta = 0.2$, $\theta^0 = 30°$.They are the monochromatic snapshots for conventional finite-difference operators (a) and weighting-averaging finite-difference operators (b). The frequency is 40Hz. Others are the snapshots in time-domain for conventional finite-difference operators (c) and weighting-averaging finite-difference operators (d). In these figures, the qP wavefront in elliptical anisotropic media is elliptical.

anisotropic features and is neither circular nor elliptical, no matter whether conventional finite-difference operators or weighting-averaging finite-difference operators are used. In the monochromatic snapshots for conventional finite-difference operators and weighting-averaging finite-difference operators, the wavefields are very similar. However, in the snapshots in the time-domain using conventional finite-differences, there are many wavefronts, which are caused by numerical dispersion. In the snapshots in the time domain using weighting-averaging finite-differences on 25-point stencils, there is one intact wavefront. It shows that weighted-averaging finite-differences on 25-point stencils reduce the numerical dispersion in a quite efficient manner.

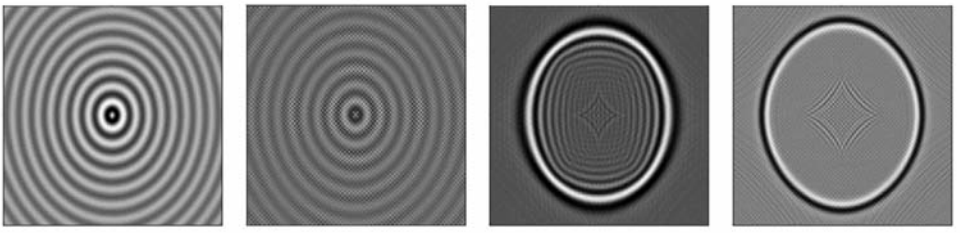

Fig. 8. The snapshots in TTI media A. The parameters are $V_{P0} = 2500$ m/s, $\varepsilon = 0.2$, $\delta = 0.1$, $\theta^0 = 90°$. They are the monochromatic snapshots for conventional finite-difference operators (a) and weighting-averaging finite-difference operators (b). The frequency is 40 Hz. Others are the snapshots in time-domain for conventional finite-difference operators (c) and weighting-averaging finite-difference operators (d). In these figures, the qP wavefront demonstrates anisotropic features and is neither circular nor elliptical.

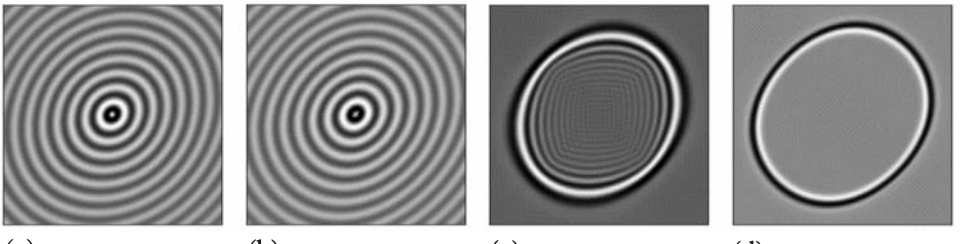

Fig. 9. The snapshots in TTI media B. The parameters are $V_{P0} = 2500$ m/s, $\varepsilon = 0.2$, $\delta = 0.3$, $\theta^0 = -45°$. They are the monochromatic snapshots for conventional finite-difference operators (a) and weighting-averaging finite-difference operators (b). The frequency is 40 Hz. Others are the snapshots in time-domain for conventional finite-difference operators (c) and weighting-averaging finite-difference operators (d). In these figures, the qP wavefront also demonstrates anisotropic features.

To study the TTI media B further, we design a set of homogeneous TTI B media with the same velocity V_{P0} and anisotropic parameters, but different values of θ^0. The tilted angle θ^0 has the values of 0°, 30°, 90°, and −45°. The snapshots in the TTI media B with $\theta^0 = 0°$, 30°, 90° and −45° are shown in Figs. 10 (a) to (d), respectively. In Fig. 10 the wavefronts in the four TTI media are similar, and show anisotropic features, except for the symmetry axis. The angle between symmetry axis of the wavefront in TTI media and the vertical axis equals θ^0, which is in good agreement with the theory. The result of numerical simulation shows the numerical dispersion is almost completely removed by weighted-averaging finite-difference operators defined on a 25-point stencil.

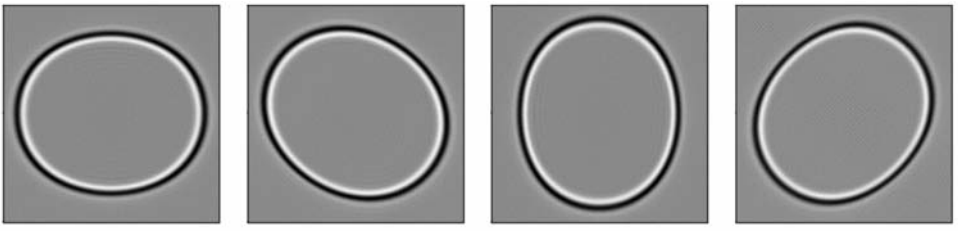

(a) (b) (c) (d)

Fig. 10. The snapshots in a set of TTI media B with the same velocity V_{P0} and anisotropic parameters, but different values of $\theta°$. The tilted angle $\theta°$ has the values of 0°, 30°, 90° and −45°, corresponding to (a) to (d), respectively. The wavefronts in the four TTI media are similar, except for the symmetry axis.

To examine the effect of TTI media on the qP wave propagation and synthetic seismograms, we simulate the qP wave propagation in layered TTI media using the weighted-averaging finite-differences on 25-point stencils. The anisotropic parameters of the layered TTI media are listed in Table 2. The first and the last layer are isotropic media, the third layer is a VTI medium, and the second layer is a TTI medium with $\theta^0 = 0°$ (degenerate into VTI media), $\theta^0 = 45°$, and $\theta^0 = -45°$. The grid dimension of the model is 201 × 101, with spatial intervals of $\Delta x = 10$ m and $\Delta z = 10$ m. The dominant frequency of the Ricker wavelet is 40 Hz. The time sample rate is 2 ms. The source is placed at the top of model. Figs. 11 and 12 show the snapshots and synthetic seismograms for the layered TTI media: (a) $\theta^0 = 0°$ (degenerate into VTI media), (b) $\theta^0 = 45°$ and (c) $\theta^0 = -45°$. In Fig. 11a, all the wavefronts are symmetric including the direct wave, reflected wave, and transmitted wave, so that all events are also symmetric in Fig. 12a, because both the isotropic media and VTI

media have vertical symmetry axes. But in Fig. 11b and 11c, the wavefronts are not symmetric except in the first layer, because the second layer is a TTI medium. The energies of corresponding reflections from the second and the third reflector are asymmetric (Figs. 12b and 12c), because the TTI medium has a tilted symmetry axis. In addition, the numerical dispersion is also almost completely removed in Figs. 11 and 12.

Table 2. Anisotropic parameters of the layered TTI media.

Layer	Depth (m)	V_{P0} (m/s)	ε	δ	θ^0
1	300	2500	0.0	0.0	0°
2	500	2900	0.2	0.3	0°/45°/−45°
3	800	3300	0.189	0.204	0°
4	1000	3700	0.0	0.0	0°

Using the weighted-averaging operators, we simulate qP wave propagation in a VTI Salt model. The anisotropy of the VTI Salt model is characterized by Thomsen's parameters which are linear functions of the perturbation of the qP velocity in this model (Han and Wu, 2004), i.e.,

$$\varepsilon(x,z) = 0.485[V_{P0}(x,z) - V_{P0min}]/V_{P0max} \ ,$$

$$\delta(x,z) = 0.606[V_{P0}(x,z) - V_{P0min}]/V_{P0max} \ .$$

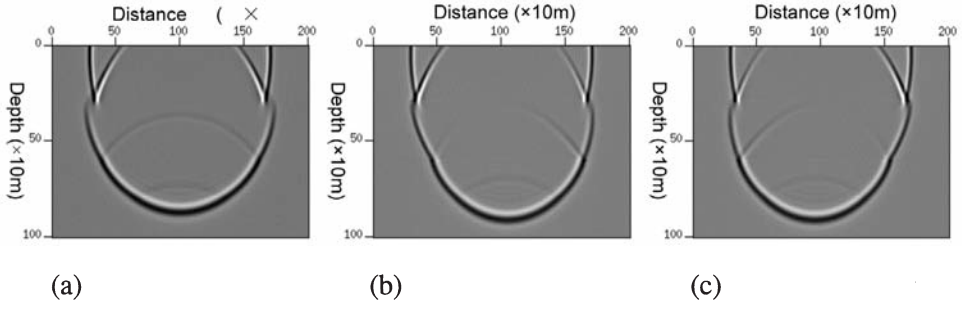

(a) (b) (c)

Fig. 11. Snapshots for the layered TTI media: the first and the last layer are isotropic media, the third layer is layer is a VTI medium, and the second layer is a TTI medium with (a) $\theta^\circ = 0^\circ$ (degenerate into VTI media), (b) $\theta^0 = 45^\circ$, and (c) $\theta^0 = -45^\circ$. All the wavefronts are symmetric in (a), and are not symmetric except in the first layer in (b) and (c).

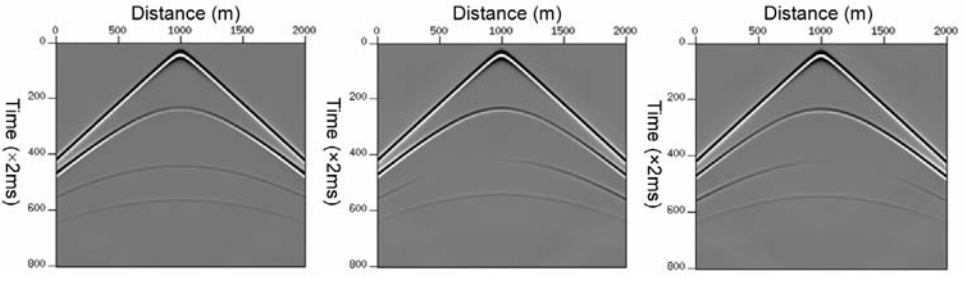

Fig. 12. Synthetic seismograms for the layered TTI media. All the energies of events are symmetric in (a), and asymmetric except in the first layer in (b) and (c).

Fig. 13 shows the VTI Salt model. The salt body is an area of high velocity and isotropy. The grid dimension of the model is 1290 × 300, with spatial intervals of $\Delta x = 10$ m and $\Delta z = 5$ m. The dominant frequency of the Ricker wavelet is 20 Hz and the time sample rate is 2 ms. The source is placed at three positions (denoted by stars in Fig. 13). Fig. 14 shows the synthetic seismograms for the VTI Salt model with different source positions. There events that may be seen in the synthetic seismograms are the direct wave, the primary reflected wave and multiply reflected and/or refracted waves due to the complexity of the model. The result of numerical simulation can lay the foundation for qP wave migration in VTI media. Fig. 15 shows pre-stack depth migration results using the Born approximation migration method for qP wave in a VTI media (Liang et al, 2008). The reflections are correctly imaged and the scattering wave is convergent because anisotropy is taken into consideration.

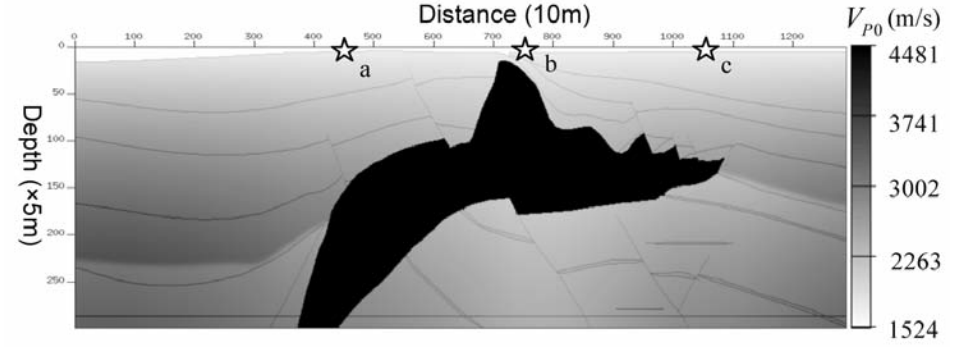

Fig. 13. Velocity model of the VTI Salt model. The salt body is an area of high velocity and isotropy. The anisotropy of the VTI Salt model is characterized by Thomsen's parameters which are linear functions of the perturbation of the qP velocity in this model the stars are the positions of the source locations: (a) $s_x = 4500$ m, (b) $s_x = 7500$ m, and (c) $s_x = 10500$ m.

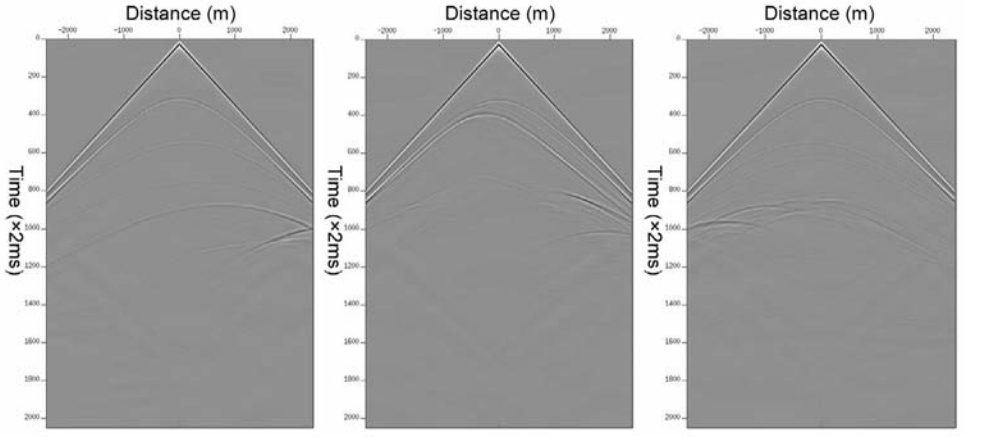

Fig. 14. Synthetic seismograms for the VTI Salt model, observed on the surface for source locations of (a) s_x = 4500 m, (b) s_x = 7500 m, and (c) s_x = 10500 m. Three events that may be seen in the synthetic seismograms are the direct wave, the primary reflected wave and multiply reflected and/or refracted waves due to the complexity of the model.

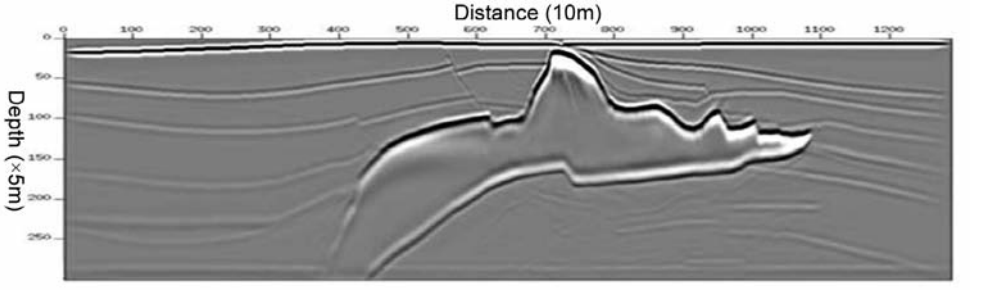

Fig. 15. Common shot pre-stack depth migration profile for the VTI Salt model using the Born approximation migration method for qP wave in a VTI media (Liang et al., 2008). The reflections are correctly imaged and the scattering wave is convergent because anisotropy is taken into consideration.

CONCLUSIONS

The finite-difference method has the problem of numerical dispersion which reduces the accuracy and resolution of seismic wavefield simulation. In order to decrease the numerical dispersion, this paper presents frequency-domain

weighted-averaging finite-differences on 25-point stencil operators for the numerical simulation of qP wave propagation in TTI media. Using the weighted-averaging operators defined on 25-point stencils, we simulate the qP wave propagation in homogeneous, layered TTI media and a VTI Salt model successfully. The result of numerical simulation, which can lay the foundation for qP wave migration and inversion in TTI media, indicates that weighted-averaging finite-difference operators defined on 25-point stencils improve the accuracy of wavefield numerical simulation, and efficiently reduce the numerical dispersion of conventional difference operators.

ACKNOWLEDGEMENTS

We would like to thank the anonymous reviewers and the editor for their valuable comments. This research is supported by the National Basic Research Program of China (973 Program) (No. 2007CB209605), and the NSFC grants No. 40739908.

REFERENCES

Alkhalifah, T., 1998. Acoustic approximation for processing in transversely isotropic media. Geophysics, 63: 623-631.

Alkhalifah, T., 2000. An acoustic wave equation for anisotropic media. Geophysics, 65: 1239-1250.

Alkhalifah, T., 2003. An acoustic wave equation for orthorhombic media. Geophysics, 68: 1169-1172.

Han, Q.Y. and Wu, R.S., 2004. Depth imaging in strongly heterogeneous VTI media. Expanded Abstr., 74th Ann. Internat. SEG Mtg., Denver: P1061-1064.

Jo, C.H., Shin, C. and Suh, J.H., 1996. An optimal 9-point, finite-difference, frequency-space, 2-D scalar wave extrapolator. Geophysics, 61: 529-537.

Komatitsch, D. and Tromp, J., 2003. A perfectly matched layer absorbing boundary condition for the second-order seismic wave equation. Geophys. J. Internat., 154: 146-153.

Liang, K., Wu, G.C. and Yin, X.Y., 2008. Born approximation migration method of qP wave in VTI media. J. Seismic Explor., 17: 169-180.

Lines, L.R. and Treitel, S., 1984. A review of least-squares inversion and its application to geophysical problems. Geophys. Prosp., 32: 159-186.

Min, D.J., Shin, C., Kwon, B.D. and Chung, S., 2000. Improved frequency-domain elastic wave modeling using weighted- averaging difference operators. Geophysics, 65: 884-895.

Min, D.J., Yoo, H.S., Shin, C., Hyun, H.J. and Suh, J.H., 2002. Weighted-averaging finite-element method for scalar wave equation in the frequency domain. J. Seismic Explor., 11: 197-222.

Min, D.J., Shin, C., Pratt, R.G. and Yoo, H.S., 2003. Weighted-averaging finite-element method for 2D elastic wave equations in the frequency domain. Bull. Seismol. Soc. Am., 93: 904-921.

Pratt, R.G., 1990. Frequency-domain elastic wave modeling by finite differences: A tool for crosshole seismic imaging. Geophysics, 55: 626-632.

Shin, C. and Sohn, H., 1998. A frequency-space 2-D scalar wave extrapolator using extend 25-point finite-difference operator. Geophysics, 63: 289-296.

Štekl, I. and Pratt, R.G., 1998. Accurate viscoelastic modeling by frequency-domain finite differences using rotated operators. Geophysics, 63: 1779-1794.

Thomsen, L,. 1986. Weak elastic anisotropy. Geophysics, 51: 1954-1966.
Wu, G.C. and Liang, K., 2005. Quasi P-wave forward modeling in frequency-space domain in VTI media. Oil Geophys. Prosp., 40: 535-545.
Wu, G.C. and Liang, K., 2005. Combined boundary conditions of quasi-P wave within frequency-space domain in VTI media. Geophys. Prosp. for Petrol., 44: 301-307.
Zeng, Y.Q., He, J.Q. and Liu, Q.H., 2001. The application of the perfectly matched layer in numerical modeling of wave propagation in poroelastic media. Geophysics, 66: 1258-1266.
Zhang, L.B., Rector III, J.W. and Hoversten, G.M., 2003. An acoustic wave equation for modeling in tilted TI media. Expanded Abstr., 73rd Ann. Internat. SEG Mtg., Dallas: P153-156.

APPENDIX

2-D frequency-domain difference equation for the qP wave

According to eq. (12) and introducing the body force vector $\boldsymbol{G}$, we get the matrix equation

$$\boldsymbol{A}_{N\times N}\boldsymbol{F} = \boldsymbol{G} \ , \tag{A-1}$$

where

$$\boldsymbol{F} = (F_{0,0}, F_{0,1}, \cdots, F_{0,Nx-1}, F_{1,0}, F_{1,1}, \cdots, F_{1,Nx-1}, \cdots\cdots, F_{Nz-1,0}, F_{Nz-1,1}, \cdots, F_{Nz-1,Nx-1})^{\mathrm{T}} ,$$

$$\boldsymbol{G} = (G_{0,0}, G_{0,1}, \cdots, G_{0,Nx-1}, G_{1,0}, G_{1,1}, \cdots, G_{1,Nx-1}, \cdots\cdots, G_{Nz-1,0}, G_{Nz-1,1}, \cdots, G_{Nz-1,Nx-1})^{\mathrm{T}} ,$$

$$\boldsymbol{A}_{N\times N} = \begin{bmatrix}
\boldsymbol{L}_0^0 & \boldsymbol{L}_1^1 & \boldsymbol{L}_2^2 & & & & & \\
\boldsymbol{L}_0^{-1} & \boldsymbol{L}_1^0 & \boldsymbol{L}_2^1 & \boldsymbol{L}_3^2 & & & & \\
\boldsymbol{L}_0^{-2} & \boldsymbol{L}_1^{-1} & \boldsymbol{L}_2^0 & \boldsymbol{L}_3^1 & \boldsymbol{L}_4^2 & & & \\
 & \boldsymbol{L}_1^{-2} & \boldsymbol{L}_2^{-1} & \boldsymbol{L}_3^0 & \boldsymbol{L}_4^1 & \boldsymbol{L}_5^2 & & \\
 & & \cdots & \cdots & \cdots & \cdots & \cdots & \\
 & & & \boldsymbol{L}_{Nz-5}^{-2} & \boldsymbol{L}_{Nz-4}^{-1} & \boldsymbol{L}_{Nz-3}^{0} & \boldsymbol{L}_{Nz-2}^{1} & \boldsymbol{L}_{Nz-1}^{2} \\
 & & & & \boldsymbol{L}_{Nz-4}^{-2} & \boldsymbol{L}_{Nz-3}^{-1} & \boldsymbol{L}_{Nz-2}^{0} & \boldsymbol{L}_{Nz-1}^{1} \\
 & & & & & \boldsymbol{L}_{Nz-3}^{-2} & \boldsymbol{L}_{Nz-2}^{-1} & \boldsymbol{L}_{Nz-1}^{0}
\end{bmatrix}$$

and

$$L_i^k = \begin{bmatrix}
A_{i,0}^{S0} & A_{i,1}^{S0+S1} & A_{i,2}^{S0+2S1} & & & & & & \\
A_{i,0}^{S0+S2} & A_{i,1}^{S0} & A_{i,2}^{S0+S1} & A_{i,3}^{S0+2S1} & & & & & \\
A_{i,0}^{S0+2S2} & A_{i,1}^{S0+S2} & A_{i,2}^{S0} & A_{i,3}^{S0+S1} & A_{i,4}^{S0+2S1} & & & & \\
 & A_{i,1}^{S0+2S2} & A_{i,2}^{S0+S2} & A_{i,3}^{S0+S0} & A_{i,4}^{S0+S1} & A_{i,5}^{S0+2S1} & & & \\
 & & \cdots & \cdots & \cdots & \cdots & \cdots & & \\
 & & & A_{i,Nx-5}^{S0+2S2} & A_{i,Nx-4}^{S0+S2} & A_{i,Nx-3}^{S0} & A_{i,Nx-2}^{S1} & A_{i,Nx-1}^{2S1} & \\
 & & & & A_{i,Nx-4}^{S0+2S2} & A_{i,Nx-3}^{S0+S2} & A_{i,Nx-2}^{S0} & A_{i,Nx-1}^{S1} & \\
 & & & & & A_{i,Nx-3}^{S0+2S2} & A_{i,Nx-2}^{S0+S2} & A_{i,Nx-1}^{S0} &
\end{bmatrix},$$

for k = −2,−1,0,1,2. The subscripts in the above matrix equation are given by

$$S0 = 5 * |k|,\ S1 = \begin{cases} \text{sign(k)} & k = -2,-1,,1,2 \\ 1 & k = 0 \end{cases}$$

and

$$S2 = \begin{cases} -\text{sign(k)} & k = -2,-1,,1,2 \\ 1 & k = 0 \end{cases}$$

and the A_{ij} are

$$A_{i,j}^{12} = (b_3d/4)(A_{i,j}+B_{i,j}) + (f_1/4)C_{i,j} + (f_2/16)D_{i,j} + g_3(E_{i,j}+G_{i,j}) + a_6\omega^4,$$

$$A_{i,j}^{11} = b_3cA_{i,j} + (b_2d/4)B_{i,j} - 4g_3E_{i,j} + g_2G_{i,j} + hI_{i,j} + a_5\omega^4,$$

$$A_{i,j}^{10} = -2b_3(c+d/4)A_{i,j} + (b_1d/4)B_{i,j} + 6g_3E_{i,j} + g_1G_{i,j} + a_4\omega^4,$$

$$A_{i,j}^{9} = b_3cA_{i,j} + (b_2d/4)B_{i,j} - 4g_3E_{i,j} + g_2G_{i,j} - hI_{i,j} + a_5\omega^4,$$

$$A_{i,j}^{8} = (b_3d/4)(A_{i,j}+B_{i,j}) - (f_1/4)C_{i,j} + (f_2/16)D_{i,j} + g_3(E_{i,j}+G_{i,j}) + a_6\omega^4,$$

$$A_{i,j}^{7} = (b_2d/4)A_{i,j} + b_3cB_{i,j} + g_2E_{i,j} - 4g_3G_{i,j} + hH_{i,j} + a_5\omega^4,$$

$$A_{i,j}^{6} = b_2c(A_{i,j}+B_{i,j}) + e_1C_{i,j} + e_2D_{i,j} - 4g_2(E_{i,j}+G_{i,j}) - 2h(H_{i,j}+I_{i,j}) + a_3\omega^4,$$

$$A_{i,j}^{5} = -2b_2(c+d/4)A_{i,j} + b_1cB_{i,j} - 2e_2D_{i,j} + 6g_2E_{i,j} - 4g_1G_{i,j} + a_2\omega^4,$$

$$A_{i,j}^{4} = b_2c(A_{i,j}+B_{i,j}) - e_1C_{i,j} + e_2D_{i,j} - 4g_2(E_{i,j}+G_{i,j}) + 2h(H_{i,j}+I_{i,j}) + a_3\omega^4,$$

$$A^3_{i,j} = (b_2 d/4)A_{i,j} + b_3 c B_{i,j} + g_2 E_{i,j} - 4g_3 G_{i,j} - hH_{i,j} + a_5\omega^4 ,$$

$$A^2_{i,j} = (b_1 d/4)A_{i,j} - 2b_3(c+d/4)B_{i,j} - (f_2/8)D_{i,j} + g_1 E_{i,j} + 6g_3 G_{i,j} + a_4\omega^4 ,$$

$$A^1_{i,j} = b_1 c A_{i,j} - 2b_2(c+d/4)B_{i,j} - 2e_2 D_{i,j} - 4g_1 E_{i,j} + 6g_2 G_{i,j} + a_2\omega^4 ,$$

$$A^0_{i,j} = -2b_3(c+d/4)(A_{i,j}+B_{i,j}) + (4e_2 + f_2/4)D_{i,j} + 6g_1(E_{i,j} + G_{i,j}) + a_1\omega^4 .$$

Dispersion relation of difference equation

According to eq. (1) and the weighted-averaging finite differences on a 25-point stencil, we have

$$\omega^2 = -\frac{V_{P0}^2}{2\Delta^2 P_m} AP_{xx} - \frac{V_{P0}^2}{2\Delta^2 P_m} BP_{zz} - \frac{V_{P0}^2}{2\Delta^2 P_m} CP_{xz} \pm \frac{V_{P0}^2}{2\Delta^2 P_m}\sqrt{M'} \qquad \text{(A-2)}$$

where

$$M' = \left(AP_{xx} + BP_{zz} + CP_{xz}\right)^2 - 4P_m\left(DP_{xxzz} + EP_{xxxx} + GP_{zzzz} + HP_{xxxz} + IP_{xzzz}\right)$$

$$P_m = a_1 + 2a_2[\cos(\frac{2\pi}{L}\sin\theta) + \cos(\frac{2\pi}{L}\cos\theta)] + 4a_3\cos(\frac{2\pi}{L}\sin\theta)\cos(\frac{2\pi}{L}\cos\theta) +$$
$$2a_4[\cos(\frac{4\pi}{L}\sin\theta) + \cos(\frac{4\pi}{L}\cos\theta)] + 4a_6\cos(\frac{4\pi}{L}\sin\theta)\cos(\frac{4\pi}{L}\cos\theta) +$$
$$4a_5[\cos(\frac{4\pi}{L}\sin\theta)\cos(\frac{2\pi}{L}\cos\theta) + \cos(\frac{2\pi}{L}\sin\theta)\cos(\frac{4\pi}{L}\cos\theta)]$$

$$P_{xx} = -\left[b_1 + 2b_2\cos(\frac{2\pi}{L}\cos\theta) + 2b_3\cos(\frac{4\pi}{L}\cos\theta)\right]\left[4c\sin^2(\frac{\pi}{L}\sin\theta) + d\sin^2(\frac{2\pi}{L}\sin\theta)\right]$$

$$P_{zz} = -\left[b_1 + 2b_2\cos(\frac{2\pi}{L}\sin\theta) + 2b_3\cos(\frac{4\pi}{L}\sin\theta)\right]\left[4c\sin^2(\frac{\pi}{L}\cos\theta) + d\sin^2(\frac{2\pi}{L}\cos\theta)\right]$$

$$P_{xz} = -e_1\sin(\frac{2\pi}{L}\sin\theta)\sin(\frac{2\pi}{L}\cos\theta) - \frac{f_1}{4}\sin(\frac{4\pi}{L}\sin\theta)\sin(\frac{4\pi}{L}\cos\theta)$$

$$P_{xxzz} = 4e_2\left[1-\cos(\frac{2\pi}{L}\sin\theta)\right]\left[1-\cos(\frac{2\pi}{L}\cos\theta)\right]+\frac{f_2}{4}\left[1-\cos(\frac{4\pi}{L}\sin\theta)\right]\left[1-\cos(\frac{4\pi}{L}\cos\theta)\right]$$

$$P_{xxxx} = -4\left[4\sin^2(\frac{\pi}{L}\sin\theta)-\sin^2(\frac{2\pi}{L}\sin\theta)\right]\left[g_1+2g_2\cos(\frac{2\pi}{L}\cos\theta)+2g_3\cos(\frac{4\pi}{L}\cos\theta)\right]$$

$$P_{zzzz} = -4\left[4\sin^2(\frac{\pi}{L}\cos\theta)-\sin^2(\frac{2\pi}{L}\cos\theta)\right]\left[g_1+2g_2\cos(\frac{2\pi}{L}\sin\theta)+2g_3\cos(\frac{4\pi}{L}\sin\theta)\right]$$

$$P_{xxxz} = h\left[2\sin(\frac{2\pi}{L}\sin\theta)\sin(\frac{2\pi}{L}\cos\theta)-\sin(\frac{4\pi}{L}\sin\theta)\sin(\frac{2\pi}{L}\sin\theta)\right]$$

$$P_{xzzz} = h\left[2\sin(\frac{2\pi}{L}\sin\theta)\sin(\frac{2\pi}{L}\cos\theta)-\sin(\frac{2\pi}{L}\sin\theta)\sin(\frac{4\pi}{L}\cos\theta)\right].$$